A DISCRETE ORDINATES SOLVER WITH DIFFUSION SYNTHETIC ACCELERATION FOR SIMULATIONS OF 2-D AND 2-ENERGY GROUP NEUTRON NOISE PROBLEMS

Huaiqian Yi[1], Paolo Vinai[1], and Christophe Demazière[1]

[1]Division of Subatomic and Plasma Physics, Department of Physics,
Chalmers University of Technology
412 96 Gothenburg, Sweden

huaiqian@chalmers.se, vinai@chalmers.se, demaz@chalmers.se

ABSTRACT

A neutron transport solver for 2-D, 2-energy-group neutron noise problems is presented. The simulator allows to determine: 1) the static neutron flux associated with a critical system; 2) the neutron noise in the frequency domain, according to a prescribed perturbation of the critical system. The perturbation is modeled as stationary fluctuations of the macroscopic nuclear cross-sections. The solution algorithm is based on a diamond finite difference scheme, discrete ordinates method, and it is accelerated using a diffusion synthetic acceleration technique. The solver is tested on 2-D homogeneous and heterogeneous systems with a localized neutron noise source. Its convergence is analyzed and compared to the case without acceleration.

KEYWORDS: Reactor neutron noise, discrete ordinates, diffusion synthetic acceleration, convergence analysis

1. INTRODUCTION

During normal, steady-state operations of a nuclear reactor, neutron flux measurements show fluctuations around mean values. These fluctuations referred to as neutron noise, may be due to a variety of perturbations such as mechanical vibrations of core internals, disturbances in the coolant flow, etc. From the analysis of the neutron noise, anomalous patterns can be identified at an early stage, so that appropriate actions can be taken before dangerous situations arise. Neutron noise-based monitoring subsequently contributes to enhanced safety. For this purpose, the reactor transfer function, which describes the core response to any possible perturbation, is most often required. The modelling of reactor transfer function can be based on the neutron transport equation, while the possible perturbations are expressed in terms of changes in the macroscopic nuclear cross-sections. Most of the past work in this area relies on neutron diffusion theory [1]. However, recent efforts focus on the development of advanced computational capabilities in order to provide more detailed simulations and to assess the limitations of the diffusion approximation for neutron noise applications [2, 3, 4].

At Chalmers University of Technology, a frequency-domain neutron noise simulator is under development. The tool is based on a discrete ordinates method and its current version can deal with two-dimensional, two-energy group problems. For the acceleration of the algorithm a diffusion synthetic acceleration technique is used. In this paper, the solver is introduced and its convergence is investigated via both a Fourier analysis and numerical tests in homogeneous and heterogeneous systems.

2. DISCRETE ORDINATES NEUTRON NOISE SOLVER

The neutron noise simulator consists of a static and dynamic module. The first module solves the criticality problem and provides the static angular and scalar neutron flux and the effective multiplication factor (with scattering treated as isotropic). The dynamic module calculates the amplitude and the phase of the neutron noise according to the prescribed neutron noise source and the estimated static solution. The dynamic simulation is performed in the frequency domain and is based on:

$$\left[\hat{\Omega}\cdot\nabla+\Sigma_{t,g,0}\left(\vec{r}\right)+\frac{i\omega}{v_g}\right]\delta\psi_g\left(\vec{r},\hat{\Omega},\omega\right)=\frac{1}{4\pi}\sum_{g'}\Sigma_{s,g'\to g,0}\left(\vec{r}\right)\delta\phi_{g'}\left(\vec{r},\omega\right)$$
$$+\frac{1}{4\pi k_{eff}}\left[\chi_{p,g}\left(\vec{r}\right)\left(1-\sum_q\beta_q\left(\vec{r}\right)\right)+\sum_q\chi_{d,g,q}\left(\vec{r}\right)\frac{\lambda_q\beta_q\left(\vec{r}\right)}{i\omega+\lambda_q}\right]\sum_{g'}\nu\Sigma_{f,g',0}\left(\vec{r}\right)\delta\phi_{g'}\left(\vec{r},\omega\right)+S_g\left(\vec{r},\hat{\Omega},\omega\right) \quad (1)$$

with the noise source expressed as:

$$S_g\left(\vec{r},\hat{\Omega},\omega\right)=-\delta\Sigma_{t,g}\left(\vec{r},\omega\right)\psi_{g,0}\left(\vec{r},\hat{\Omega}\right)+\frac{1}{4\pi}\sum_{g'}\delta\Sigma_{s,g'\to g}\left(\vec{r},\omega\right)\phi_{g',0}\left(\vec{r}\right)$$
$$+\frac{1}{4\pi k_{eff}}\left[\chi_{p,g}\left(\vec{r}\right)\left(1-\sum_q\beta_q\left(\vec{r}\right)\right)+\sum_q\chi_{d,g,q}\left(\vec{r}\right)\frac{\lambda_q\beta_q\left(\vec{r}\right)}{i\omega+\lambda_q}\right]\sum_{g'}\nu\delta\Sigma_{f,g'}\left(\vec{r},\omega\right)\phi_{g',0}\left(\vec{r}\right) \quad (2)$$

Eq. (1) represents a fixed source problem and is derived from the time-dependent, multi-group neutron transport equation with a generic number of families of precursors of delayed neutrons. The derivation process is similar to the procedure described in [4], and is briefly summarized in the following.

Small, stationary perturbations of the macroscopic nuclear cross-sections are assumed, while the other system parameters including the effective multiplication factor are kept constant. In the time-dependent equation, the neutron flux, the concentration of precursors and the cross-sections are separated into the sum of a static mean value and a fluctuating part. The static equation is then subtracted from the time-dependent equation, so that the mean values are removed. A temporal Fourier transform is performed, and the second-order perturbation terms are neglected (i.e., linear theory is applied). The notation for Eq. (1) is standard; $\delta\psi_g$ and $\delta\phi_g$ are the induced angular and scalar neutron noise respectively, and $\omega=2\pi f$ is the angular frequency of the driving perturbation and i is the imaginary unit.

The energy discretization is limited to two energy groups and up-scattering is neglected. A diamond difference scheme is used for the spatial discretization of the equations, and a discrete ordinates method is used for the angular discretization. In the static module, the common set-to-zero negative flux fixup approach is used. The mesh boundary angular fluxes are set to zero if negative values are computed and the neutron balance equation is re-evaluated with the newly assigned boundary values. The dynamic module does not require any fixup for negative fluxes, because it calculates the neutron noise as a complex quantity in the frequency domain.

According to the typical numerical procedure for the solution of the multi-group neutron transport equation, inner with-in group scattering iterations are carried out per each of the outer fission source iterations. A Diffusion Synthetic Acceleration (DSA) is implemented in both the static and dynamic modules for reducing the number of both the inner and the outer iterations, and thus enhancing the convergence rate of the overall algorithm.

In case of the static solver, the derivation and implementation of the DSA equations is based on the work reported in [5]. Tests of the accelerated static algorithm were carried out and satisfactory performances in the reduction of both inner and outer iteration were obtained. A similar procedure is followed for the

acceleration of the dynamic solver. In this case the main difference with the static calculations is that a fixed source problem needs to be accelerated since only the fission source is updated in the outer iterations and k_{eff} is assumed to be unchanged. The basics of the unaccelerated and accelerated version of the dynamic module is discussed below.

Arranging Eq. (1) in a matrix form, the two-energy group, angular neutron noise column-vector $\boldsymbol{\delta\psi}^{(l,m+1/2)}$ (where m and l denote the inner and outer iteration indexes respectively) is estimated from the equation associated with the transport sweep:

$$\begin{aligned}&\hat{\Omega}\cdot\nabla\boldsymbol{\delta\psi}^{(l,m+1/2)}\left(\vec{r},\hat{\Omega},\omega\right)+\boldsymbol{\Sigma}_{\mathbf{t}}^{\mathbf{dyn}}\left(\vec{r},\omega\right)\boldsymbol{\delta\psi}^{(l,m+1/2)}\left(\vec{r},\hat{\Omega},\omega\right)\\&=\frac{1}{4\pi}\boldsymbol{\Sigma}_{s,s}\left(\vec{r}\right)\boldsymbol{\delta\phi}^{(l,m)}\left(\vec{r},\omega\right)+\frac{1}{4\pi}\boldsymbol{\Sigma}_{s,d}\left(\vec{r}\right)\boldsymbol{\delta\phi}^{(l,M)}\left(\vec{r},\omega\right)+\frac{1}{4\pi}\boldsymbol{\chi}\left(\vec{r},\omega\right)\boldsymbol{\nu\Sigma}_{\mathbf{f}}\left(\vec{r}\right)\boldsymbol{\delta\phi}^{(l)}\left(\vec{r},\omega\right)+\mathbf{S}\left(\vec{r},\hat{\Omega},\omega\right)\end{aligned}\tag{3}$$

In Eq. (3), the definition of the matrices and vectors are:

$$\begin{aligned}&\boldsymbol{\Sigma}_{s,s}=\begin{bmatrix}\Sigma_{s,1\to1,0}&0\\0&\Sigma_{s,2\to2,0}\end{bmatrix},\ \boldsymbol{\Sigma}_{s,d}=\begin{bmatrix}0&\Sigma_{s,1\to2,0}\\0&0\end{bmatrix},\\&\boldsymbol{\Sigma}_{\mathbf{t}}^{\mathbf{dyn}}=\begin{bmatrix}\Sigma_{t,1,0}+i\omega/v_1&0\\0&\Sigma_{t,2,0}+i\omega/v_2\end{bmatrix},\ \boldsymbol{\nu\Sigma}_{\mathbf{f}}=\frac{1}{k_{eff}}\begin{bmatrix}\nu\Sigma_{f,1,0}&\nu\Sigma_{f,2,0}\end{bmatrix},\\&\boldsymbol{\chi}=\begin{bmatrix}\chi_{p,1}\left(1-\sum_q\beta_q\right)+\sum_q\chi_{d,1,q}\dfrac{\lambda_q\beta_q}{i\omega+\lambda_q}\\\chi_{p,2}\left(1-\sum_q\beta_q\right)+\sum_q\chi_{d,2,q}\dfrac{\lambda_q\beta_q}{i\omega+\lambda_q}\end{bmatrix}\end{aligned}\tag{4}$$

The right-hand side of Eq. (3) contains 4 terms. The first term that represents the self-scattering source is updated from the previous m-th inner iteration. The maximum number of inner iterations for each energy group is fixed to M. The second term $\boldsymbol{\Sigma}_{s,d}\left(\vec{r}\right)\boldsymbol{\delta\phi}^{(l,M)}\left(\vec{r},\omega\right)$ is the down-scattering; it does not give any contribution to the first energy group and it is estimated after performing the prescribed M inner iterations for the first energy group. The third term is the fission source term, and it is updated after each outer iteration. The last term is a column-vector that is related to the neutron noise source (see Eq. (2)). The angular neutron noise $\boldsymbol{\delta\psi}^{(l,m+1/2)}$ calculated from Eq. (3), is integrated over the angle $\hat{\Omega}$ in order to obtain the scalar neutron noise:

$$\boldsymbol{\delta\phi}^{(l,m+1/2)}=\int\boldsymbol{\delta\psi}^{(l,m+1/2)}d\hat{\Omega}.\tag{5}$$

In the unaccelerated algorithm, one inner iteration is completed with $\boldsymbol{\delta\phi}^{(l,m+1)}=\boldsymbol{\delta\phi}^{(l,m+1/2)}$. When M inner iterations for both groups are performed, the fission source is updated for next outer iteration:

$$\boldsymbol{\delta\phi}^{(l+1)}=\boldsymbol{\delta\phi}^{(l,M)}\tag{6}$$

In the DSA-based algorithm, the scalar neutron noise $\boldsymbol{\delta\phi}^{(l,m+1/2)}$ evaluated with Eq. (5) is introduced in the DSA equation associated with the inner iterations:

$$-\nabla\cdot\mathbf{D}\left(\vec{r},\omega\right)\nabla\mathbf{F}_{\mathbf{i}}^{(l,m+1)}\left(\vec{r},\omega\right)+\boldsymbol{\Sigma}_{\mathbf{R}}\left(\vec{r},\omega\right)\mathbf{F}_{\mathbf{i}}^{(l,m+1)}\left(\vec{r},\omega\right)=\boldsymbol{\Sigma}_{s,s}\left(\vec{r}\right)\left(\boldsymbol{\delta\phi}^{(l,m+1/2)}-\boldsymbol{\delta\phi}^{(l,m)}\right)\left(\vec{r},\omega\right),\tag{7}$$

with $\mathbf{D}=1/\left(3\boldsymbol{\Sigma}_{\mathbf{t}}^{\mathbf{dyn}}\right)$ and $\boldsymbol{\Sigma}_{\mathbf{R}}=\boldsymbol{\Sigma}_{\mathbf{t}}^{\mathbf{dyn}}-\boldsymbol{\Sigma}_{\mathbf{s,s}}$. The value of $\mathbf{F}_{\mathbf{i}}^{(l,m+1)}$ calculated for each inner iteration is used to update the estimate of $\boldsymbol{\delta\phi}^{(l,m+1)}$ via the following relationship:

$$\boldsymbol{\delta\phi}^{(l,m+1)}=\boldsymbol{\delta\phi}^{(l,m+1/2)}+\mathbf{F}_{\mathbf{i}}^{(l,m+1)}.\tag{8}$$

After M inner iterations, Eq. (8) provides $\boldsymbol{\delta\phi}^{(l,M)}$ which is needed in the DSA equation for the outer iterations:

$$\left[-\nabla\cdot\mathbf{D}\left(\vec{r},\omega\right)\nabla+\mathbf{\Sigma_R}\left(\vec{r},\omega\right)\right]\mathbf{F_o}^{(l+1)}\left(\vec{r},\omega\right)=\mathbf{\Sigma}_{s,d}\left(\vec{r}\right)\mathbf{F_o}^{(l+1)}\left(\vec{r},\omega\right)+\boldsymbol{\chi}\left(\vec{r},\omega\right)\mathbf{\nu\Sigma_f}\left(\vec{r}\right)\left(\boldsymbol{\delta\phi}^{(l,M)}-\boldsymbol{\delta\phi}^{(l)}\right)\left(\vec{r},\omega\right). \quad (9)$$

The value of $\mathbf{F_o}^{(l+1)}$ is obtained from Eq. (9) and is introduced in:

$$\boldsymbol{\delta\phi}^{(l+1)}=\boldsymbol{\delta\phi}^{(l,M)}+\mathbf{F_o}^{(l+1)}, \quad (10)$$

so that $\boldsymbol{\delta\phi}^{(l+1)}$ can be determined. The latter is sent back to Eq. (3) unless the convergence criterion is met.

Both Eqs. (7) and (9) are fixed source diffusion problems. Eq. (7) is solved for each energy group while Eq. (9) is solved for the 2 energy groups together. The spatial discretization of these equations leads to systems of linear equations. For the solution, the corresponding matrices are inverted by applying an incomplete LU factorization.

3. FOURIER CONVERGENCE ANALYSIS

For the analysis of the convergence rate of the frequency-domain dynamic solver, the spectral radius associated with the outer iteration of the algorithm is evaluated both analytically and numerically.

It was shown in [6] that the performance of the diamond-differenced DSA method is insensitive to the numbers of spatial dimensions. This is also observed in the current framework. In fact, the Fourier convergence analysis of the two-dimensional version discretized in space and angle and the one-dimensional continuous version of Eqs. (3)-(10) have given identical prediction of the convergence behavior. For simplicity, only the analytical derivation for the one-dimensional continuous case is discussed.

The analytical derivation follows the Fourier approach used, e.g., in [7] and [8]. The errors of the quantities calculated at each m- or l-th iteration of the scheme described by Eqs. (3)-(10), are denoted by the subscript err and are defined by introducing the following Fourier ansatz for each Fourier error mode Θ:

$$\boldsymbol{\delta\phi}_{err}^{(l)}\left(x,\omega,\Theta\right)=\boldsymbol{A}^{(l)}\left(\omega,\Theta\right)e^{i\Theta x} \quad (11)$$

$$\boldsymbol{\delta\psi}_{err}^{(l,m+1/2)}\left(x,\hat{\Omega},\omega,\Theta\right)=\boldsymbol{A}^{(l)}\left(\omega,\Theta\right)\boldsymbol{\alpha}^{(l,m)}\left(\hat{\Omega},\omega,\Theta\right)e^{i\Theta x} \quad (12)$$

$$\boldsymbol{\delta\phi}_{err}^{(l,m)}\left(x,\omega,\Theta\right)=\boldsymbol{A}^{(l)}\left(\omega,\Theta\right)\boldsymbol{\xi}^{(l,m)}\left(\omega,\Theta\right)e^{i\Theta x} \quad (13)$$

$$\boldsymbol{\delta\phi}_{err}^{(l,m+1/2)}\left(x,\omega,\Theta\right)=\boldsymbol{A}^{(l)}\left(\omega,\Theta\right)\boldsymbol{\beta}^{(l,m)}\left(\omega,\Theta\right)e^{i\Theta x} \quad (14)$$

$$\boldsymbol{\delta\phi}_{err}^{(l+1/2)}\left(x,\omega,\Theta\right)=\boldsymbol{A}^{(l)}\left(\omega,\Theta\right)\boldsymbol{\theta}^{(l)}\left(\omega,\Theta\right)e^{i\Theta x} \quad (15)$$

$$\mathbf{F}_{\mathbf{i},err}^{(l,m+1)}\left(x,\omega,\Theta\right)=\boldsymbol{A}^{(l)}\left(\omega,\Theta\right)\boldsymbol{\gamma}^{(l,m)}\left(\omega,\Theta\right)e^{i\Theta x} \quad (16)$$

$$\mathbf{F}_{\mathbf{o},err}^{(l+1)}\left(x,\omega,\Theta\right)=\boldsymbol{A}^{(l)}\left(\omega,\Theta\right)\boldsymbol{\vartheta}^{(l)}\left(\omega,\Theta\right)e^{i\Theta x} \quad (17)$$

where $\boldsymbol{A}$, $\boldsymbol{\alpha}$, $\boldsymbol{\beta}$, $\boldsymbol{\gamma}$, $\boldsymbol{\xi}$, $\boldsymbol{\theta}$ and $\boldsymbol{\vartheta}$ are all diagonal matrices. Eqs. (11)-(17) are used into Eqs. (3)-(10) with $\mathbf{S}\left(\vec{r},\hat{\Omega},\omega\right)=0$, so that a set of equations can be built for the errors. Eqs. (11) to (13) are inserted into Eq. (3) and the angle-independent terms are collected on the right-hand side of the resulting equation. The latter is integrated over the angle and combined with the equation:

$$\boldsymbol{\beta}^{(l,m)}\left(\omega,\Theta\right)=\int_{-1}^{1}\boldsymbol{\alpha}^{(l,m)}\left(\mu,\omega,\Theta\right) \quad (18)$$

that is derived from Eqs. (5), (12) and (14). This yield:

$$\boldsymbol{\beta}^{(l,m)}\left(\omega,\Theta\right)=\mathbf{T}\boldsymbol{\sum}_{\mathbf{t}}^{\mathbf{dyn}\ -1}\left[\mathbf{\Sigma}_{\mathbf{s,s}}\boldsymbol{\xi}^{(l,m)}+\mathbf{\Sigma}_{\mathbf{s,d}}\boldsymbol{\xi}^{(l,M)}+\boldsymbol{\chi}\mathbf{\nu\Sigma}_{\mathbf{f}}\right], \quad (19)$$

where

$$\mathbf{T}=\frac{1}{2}\int_{-1}^{1}\left(i\mu\Theta\boldsymbol{\Sigma}_{\mathbf{t}}^{\mathbf{dyn}^{-1}}+\mathbf{I}\right)d\mu\,. \tag{20}$$

Eqs. (13), (14) and (16) are used in Eq. (7) to have the following expression:

$$\boldsymbol{\gamma}^{(l,m)}(\omega,\Theta)=\left(\Theta^2\mathbf{D}+\boldsymbol{\Sigma}_{\mathbf{R}}\right)^{-1}\boldsymbol{\Sigma}_{\mathbf{s,s}}\left(\boldsymbol{\beta}^{(l,m)}(\omega,\Theta)-\boldsymbol{\xi}^{(l,m)}(\omega,\Theta)\right)=\mathbf{L}\left(\boldsymbol{\beta}^{(l,m)}(\omega,\Theta)-\boldsymbol{\xi}^{(l,m)}(\omega,\Theta)\right). \tag{21}$$

Eq. (8) with (13), (14) and (16) leads to:

$$\boldsymbol{\xi}^{(l,m+1)}(\omega,\Theta)=\boldsymbol{\beta}^{(l,m)}(\omega,\Theta)+\boldsymbol{\gamma}^{(l,m)}(\omega,\Theta). \tag{22}$$

Eqs. (19) and (21) are inserted into Eq. (22) and a recurrence relationship is found for $\boldsymbol{\xi}^{(l,m)}$:

$$\boldsymbol{\xi}^{(l,m+1)}=\mathbf{P}\boldsymbol{\xi}^{(l,m)}+\mathbf{Q}\boldsymbol{\xi}^{(l,M)}+\mathbf{R} \tag{23}$$

where

$$\begin{aligned}\mathbf{P}&=\left(\mathbf{I}+\mathbf{L}\right)\mathbf{T}\boldsymbol{\Sigma}_{\mathbf{t}}^{\mathbf{dyn}^{-1}}\boldsymbol{\Sigma}_{\mathbf{s,s}}-\mathbf{L},\\ \mathbf{Q}&=\left(\mathbf{I}+\mathbf{L}\right)\mathbf{T}\boldsymbol{\Sigma}_{\mathbf{t}}^{\mathbf{dyn}^{-1}}\boldsymbol{\Sigma}_{\mathbf{s,d}},\\ \mathbf{R}&=\left(\mathbf{I}+\mathbf{L}\right)\mathbf{T}\boldsymbol{\Sigma}_{\mathbf{t}}^{\mathbf{dyn}^{-1}}\boldsymbol{\chi}\boldsymbol{\nu}\boldsymbol{\Sigma}_{\mathbf{f}}\end{aligned} \tag{24}$$

and $\mathbf{I}$ is the identity matrix with a size equal to 2. From Eq. (23), one could demonstrate that:

$$\begin{aligned}\boldsymbol{\xi}^{(l,m)}&=\mathbf{P}^m\boldsymbol{\xi}^{(l,0)}+\left(\mathbf{P}^{m-1}+\mathbf{P}^{m-2}+\cdots+\mathbf{I}\right)\left(\mathbf{Q}\boldsymbol{\xi}^{(l,M)}+\mathbf{R}\right)\\ &=\mathbf{P}^m\boldsymbol{\xi}^{(l,0)}+\left(\mathbf{I}-\mathbf{P}\right)^{-1}\left(\mathbf{I}-\mathbf{P}^{\mathbf{m}}\right)\left(\mathbf{Q}\boldsymbol{\xi}^{(l,M)}+\mathbf{R}\right)\end{aligned}. \tag{25}$$

Since $\boldsymbol{\delta\phi}_{err}^{(l,m=0)}=\boldsymbol{\delta\phi}_{err}^{(l)}$, $\boldsymbol{\xi}^{(l,0)}$ is equal to $\mathbf{I}$ and thus the solution for $\boldsymbol{\xi}^{(l,m=M)}$ is:

$$\boldsymbol{\xi}^{(l,M)}=\left[\mathbf{I}-\left(\mathbf{I}-\mathbf{P}\right)^{-1}\left(\mathbf{I}-\mathbf{P}^{\mathbf{M}}\right)\mathbf{Q}\right]^{-1}\left[\mathbf{P}^{\mathbf{M}}+\left(\mathbf{I}-\mathbf{P}\right)^{-1}\left(\mathbf{I}-\mathbf{P}^{\mathbf{M}}\right)\mathbf{R}\right] \tag{26}$$

The maximum amplitude of the eigenvalues of the matrix on the right hand side of Eq. (26) represents the spectral radius of the outer iterations if DSA is only applied to the inner iterations. The acceleration of the outer iterations is added by inserting Eqs. (11), (13) and (17) into Eq. (9), which yields:

$$\boldsymbol{\vartheta}^{(l)}=\left(\Theta^2\mathbf{D}+\boldsymbol{\Sigma}_{\mathbf{R}}-\boldsymbol{\Sigma}_{\mathbf{s,d}}\right)^{-1}\boldsymbol{\chi}\boldsymbol{\nu}\boldsymbol{\Sigma}_{\mathbf{f}}\left(\boldsymbol{\xi}(\Theta)-\mathbf{I}\right) \tag{27}$$

Eqs. (13) and (17) are used in Eq. (10) and the following relationship is derived:

$$\boldsymbol{A}^{(l+1)}=\boldsymbol{A}^{(l)}\left(\boldsymbol{\xi}^{(l,M)}+\boldsymbol{\vartheta}^{(l)}\right) \tag{28}$$

The combination of Eqs. (26), (27) and (28), gives the expression for the spectral radius for the outer iterations when both inner and outer iterations are accelerated:

$$\rho_{DSA}(M,\omega,\Theta)=\max\left\{abs\left[eig\left(\boldsymbol{\xi}(M,\omega,\Theta)+\left(\Theta^2\mathbf{D}+\boldsymbol{\Sigma}_{\mathbf{R}}-\boldsymbol{\Sigma}_{\mathbf{s,d}}\right)^{-1}\boldsymbol{\chi}\boldsymbol{\nu}\boldsymbol{\Sigma}_{\mathbf{f}}\left(\boldsymbol{\xi}(M,\omega,\Theta)-\mathbf{I}\right)\right)\right]\right\} \tag{29}$$

The eigenvalues computed based on the matrices in Eq. (29) are complex values. Their amplitudes correspond to their absolute values, which are real and positive.

The spectral radius can also be numerically estimated by:

$$\rho_{Num}(M,\omega)=\frac{\left\|\boldsymbol{\delta\phi}^{(l+1)}(\vec{r},\omega)-\boldsymbol{\delta\phi}^{(l)}(\vec{r},\omega)\right\|_2}{\left\|\boldsymbol{\delta\phi}^{(l)}(\vec{r},\omega)-\boldsymbol{\delta\phi}^{(l-1)}(\vec{r},\omega)\right\|_2} \tag{30}$$

where $\|\cdot\|_2$ is the Euclidean norm and $\boldsymbol{\delta\phi}$ is the two-energy group scalar neutron noise column-vector computed numerically. As mentioned above, the analytical derivation in 2-D can follow a similar procedure and a similar outcome can be reached. In the next section, the discussion about the numerical results focuses on 2-D problems.

In the case of the unaccelerated scheme, the theoretical spectral radius can be derived from the procedure used for Eq. (19)-(26), but neglecting Eqs. (21) and (22). As a result, the theoretical spectral radius for the outer iterations, with M number of inner iterations per outer iteration, is expressed by the following relationship:

$$\rho(M,\omega,\Theta)=\max\left\{abs\left[eig\left(\left[\mathbf{I}-\left(\mathbf{I}-\mathbf{P}'\right)^{-1}\left(\mathbf{I}-\mathbf{P}'^{\mathbf{M}}\right)\mathbf{Q}'\right]^{-1}\left[\mathbf{P}'^{\mathbf{M}}+\left(\mathbf{I}-\mathbf{P}'\right)^{-1}\left(\mathbf{I}-\mathbf{P}'^{\mathbf{M}}\right)\mathbf{R}'\right]\right)\right]\right\} \tag{31}$$

with

$$\begin{aligned}\mathbf{P}'&=\mathbf{T}\boldsymbol{\Sigma}_{\mathbf{t}}^{\mathbf{dyn}\,-1}\boldsymbol{\Sigma}_{\mathbf{s,s}},\\ \mathbf{Q}'&=\mathbf{T}\boldsymbol{\Sigma}_{\mathbf{t}}^{\mathbf{dyn}\,-1}\boldsymbol{\Sigma}_{\mathbf{s,d}},\\ \mathbf{R}'&=\mathbf{T}\boldsymbol{\Sigma}_{\mathbf{t}}^{\mathbf{dyn}\,-1}\boldsymbol{\chi}\boldsymbol{\nu}\boldsymbol{\Sigma}_{\mathbf{f}}\end{aligned} \tag{32}$$

4. NUMERICAL RESULTS

The unaccelerated and accelerated solvers have been compared over neutron noise problems in 2-D homogeneous and heterogeneous systems.

In the case of the homogeneous configuration, the cross-section data and kinetic parameters for both groups are taken from the numerical test given in [4]. The boundary conditions are reflective on all sides. The numerical computational mesh consists of 30 × 30 square meshes each with a size of 1 × 1 cm. Level-symmetric S8 quadrature set is used. The multiplication factor computed from the static module is 1.116201 which is identical to the reference value given in [4]. The neutron noise source is defined by a stationary fluctuation of the thermal capture cross-section in one point of the system. The amplitude of the perturbation does not impact the convergence analysis and is selected equal to unity. The spectral radius is estimated both analytically using Eqs. (29) and (31), and with the numerical results of the solver via Eq. (30).

As shown in Eq. (29), the theoretical spectral radius depends on the error mode Θ. In Figure 1, the spectral radius is plotted with respect to the error mode with M set to 2 and the frequency of the calculation taken at 1 Hz (or $\omega=2\pi$ rad/s). In both the accelerated and unaccelerated cases the maximum value of the spectral radius is found for the zero-value of the error mode, that has a weak spatial dependence. The analysis is then limited to this error mode.

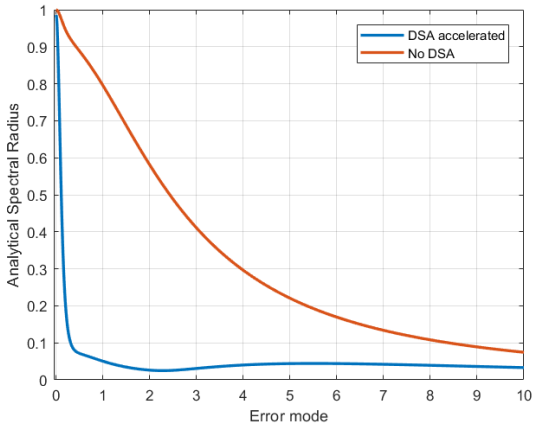

Figure 1 Spectral radius as a function of the error mode for accelerated and unaccelerated schemes

In Figure 2 the numerical and analytical spectral radius are given with respect to the number M of inner iterations per outer iteration, at frequencies 0.01 Hz and 1kHz. From the comparison, the performance of the solvers is consistent with the predictions of the theoretical approach. For the unaccelerated numerical scheme, the spectral radius decreases with more inner iterations performed.

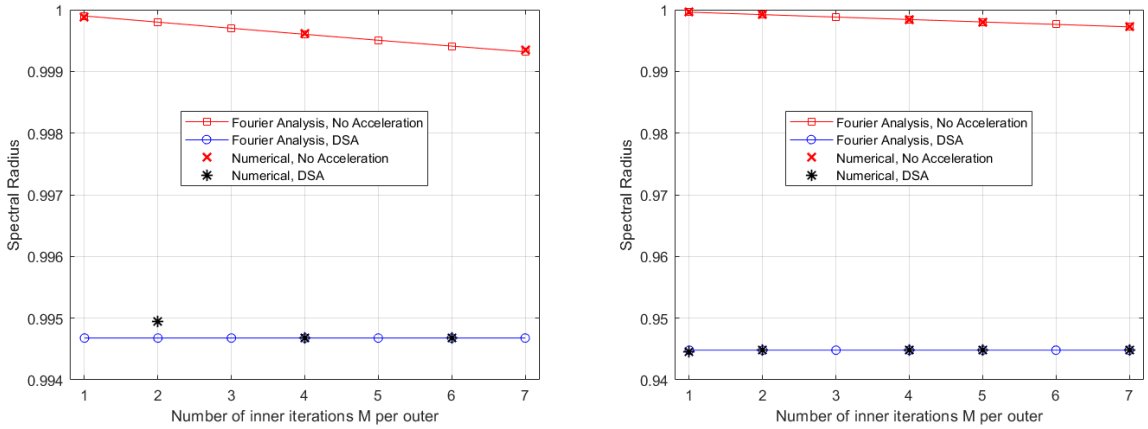

Figure 2 Spectral radius as a function of *M* for accelerated and unaccelerated schemes for frequencies of 0.01 Hz (left) and 1000 Hz (right)

For the accelerated solver, the results show that the number of inner iterations have no effect on the convergence. In fact, when the error-mode is taken to be zero, the term $\mathbf{T}$ defined in Eq. (20) becomes an identity matrix, and the matrix $\mathbf{L}$ defined in Eq. (21) is simply $\boldsymbol{\Sigma}_{\mathbf{R}}^{-1}\boldsymbol{\Sigma}_{\mathbf{s,s}}$. It can then be found from Eq. (24) that:

$$\begin{aligned}\mathbf{P} &= \left(\mathbf{I}+\boldsymbol{\Sigma}_{\mathbf{R}}^{-1}\boldsymbol{\Sigma}_{\mathbf{s,s}}\right)\boldsymbol{\Sigma}_{\mathbf{t}}^{\mathbf{dyn}^{-1}}\boldsymbol{\Sigma}_{\mathbf{s,s}}-\boldsymbol{\Sigma}_{\mathbf{R}}^{-1}\boldsymbol{\Sigma}_{\mathbf{s,s}} \\ &= \left(\mathbf{I}+\boldsymbol{\Sigma}_{\mathbf{R}}^{-1}\left(\boldsymbol{\Sigma}_{\mathbf{t}}^{\mathbf{dyn}}-\boldsymbol{\Sigma}_{\mathbf{R}}\right)\right)\boldsymbol{\Sigma}_{\mathbf{t}}^{\mathbf{dyn}^{-1}}\boldsymbol{\Sigma}_{\mathbf{s,s}}-\boldsymbol{\Sigma}_{\mathbf{R}}^{-1}\boldsymbol{\Sigma}_{\mathbf{s,s}} \\ &= 0\end{aligned} \tag{33}$$

This makes Eq. (26) and consequently the function for the spectral radius in Eq. (29) independent of M.

As the frequency decreases, the spectral radius is less influenced by the number of inner iterations associated with the unaccelerated scheme. In fact, the spectral radius decreases by about 0.06 % when M increases from 1 to 7 at 0.01 Hz and 0.24% at 1000 Hz. In addition, the effectiveness of the diffusion synthetic method also decreases.

The relationship between spectral radius and frequency of the neutron noise source is plotted in Figure 3 for both the accelerated and unaccelerated schemes with $M = 4$. The numerical behavior of the solvers is in agreement with the theoretical prediction. For both schemes, a plateau region is found between ~0.1 Hz and ~100 Hz, where the convergence is rather insensitive to the frequency. Outside the plateau region, the lower the frequency is, the less efficient the solution scheme.

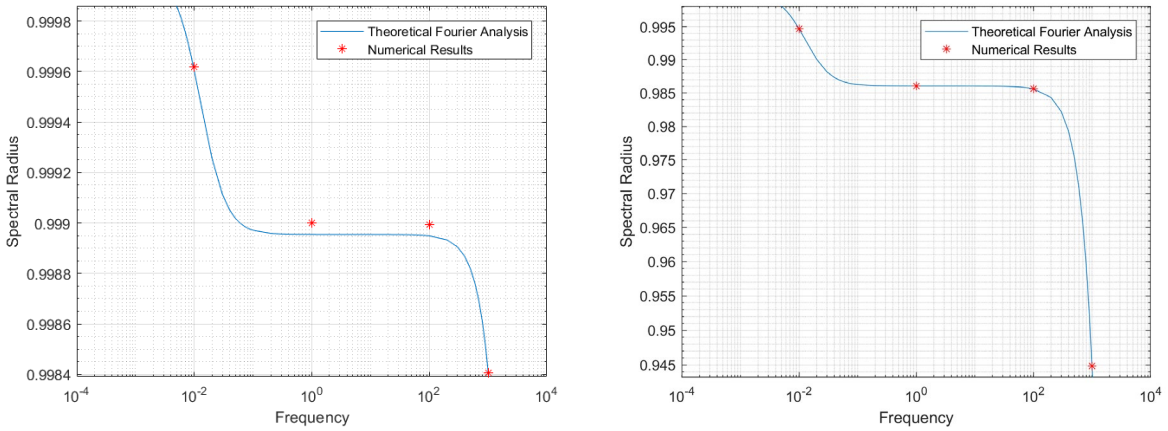

Figure 3. Spectral radius as a function of frequency for the unaccelerated scheme (left) and for the accelerated scheme (right)

The accelerated and unaccelerated solvers are further tested using two heterogeneous problems based on the two-dimensional C3 and C4V configurations reported in [9]. The C3 and C4V systems consist of a 2×2 assembly arrangement, where two UO_2 assemblies are respectively located North-West and South-East and two MOX assemblies are respectively located North-East and South-West. Each fuel assembly contains 17×17 homogenized fuel cells. The C3 test case has reflective boundary condition on all sides of the system while the C4V test case has both reflective and vacuum boundary conditions.

The neutron noise source is assumed to be a stationary fluctuation of the capture cross-section in both energy groups, placed at the fuel cell with position index (16,19) which belongs to the North-East MOX fuel assembly. The amplitude of the perturbation is taken to be 5% of the nominal values of the capture cross-section for each group. The frequency of the perturbation is set to 1 Hz.

The problems are solved with the same 34×34 mesh where each node corresponds to a homogenized fuel cell and has a size of 1.26×1.26 cm. Level-symmetric S8 quadrature sets are also used. The convergence is checked for the pointwise scalar neutron noise. Since the neutron noise calculated in the frequency domain is a complex quantity, convergence criteria are applied to the real part, the imaginary part, the amplitude and the phase of the neutron noise. The convergence is met when the relative difference between two iterations of all the quantities is lower than 1E-7.

The two problems are solved with the unaccelerated and the accelerated algorithm with one inner iteration per outer iteration. As summarized in Table I, the use of DSA reduces significantly the number of outer iterations from 30197 to 1449 for the C3 configuration, and from 29991 to 1436 for the C4V configuration. The results also show that the two solvers provide very similar predictions: the maximum relative difference in these simulations was lower than 0.03% and it was found to be in the imaginary part of the neutron noise.

Table I. Comparison of the number of outer iterations required for convergence between the diffusion synthetic accelerated and unaccelerated algorithm

Problem	Unaccelerated	Accelerated
C3	30297	1449
C4V	29991	1436

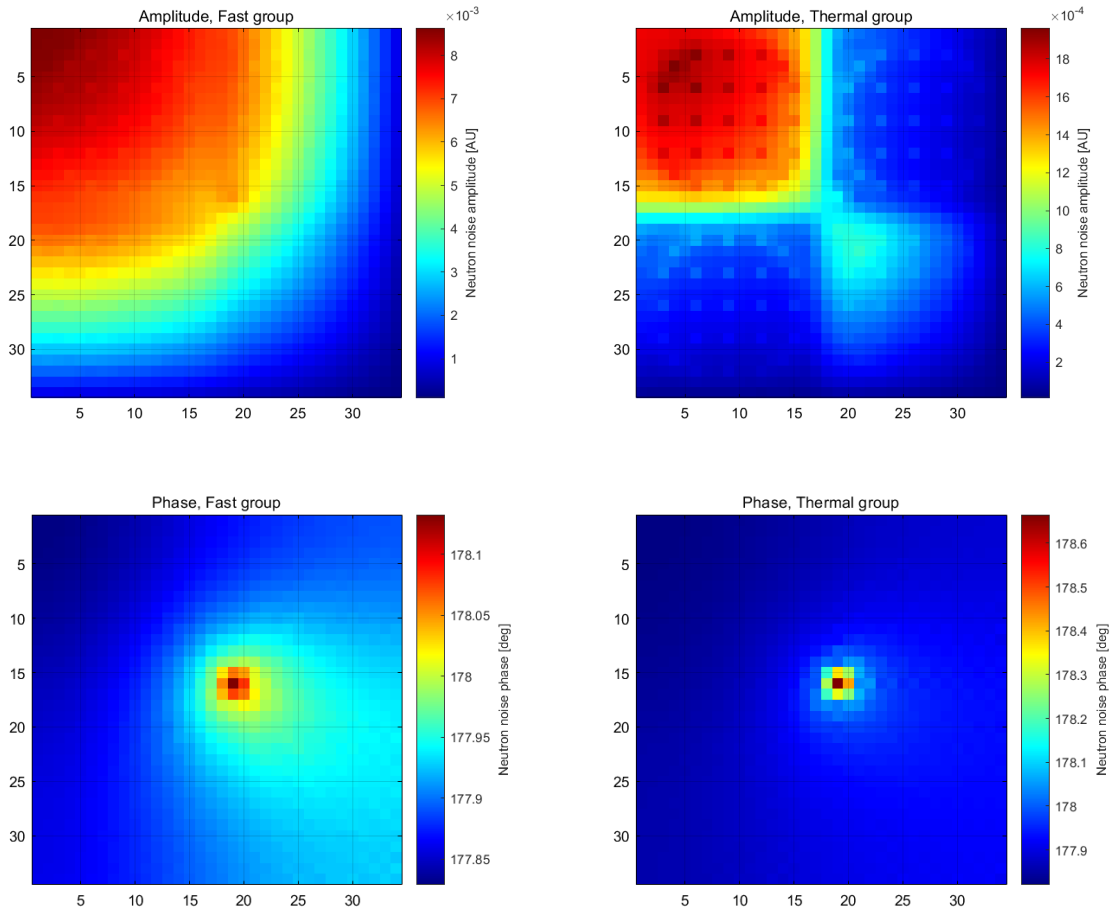

Figure 4. Amplitude and phase of the neutron noise for both groups based on the CV4 problem

The amplitude and phase of the neutron noise results for the C4V case are shown in Figure 4. The spatial distribution for the noise amplitudes in both groups follows the trend of the static flux with the exception of a local peak at the location of the noise source. The phase is, as expected, close to 180 degrees, and it decreases slightly when moving away from the source location. The decrease of phase indicates that the response of the neutron flux to the perturbation is a little delayed further away from the source. A detailed analysis of the C3 case is discussed in [10], where the neutron noise results obtained using the accelerated algorithm presented in this paper are compared to those obtained using the diffusion approximation.

5. CONCLUSIONS

A 2-dimensional neutron noise solver based on the diamond finite difference scheme, a discrete ordinates method and 2-energy group formalism was presented. The solver first estimates the static neutron flux and then the neutron noise induced by possible perturbations expressed in terms of stationary fluctuations of the macroscopic neutron cross-sections. The static and dynamic calculations were both accelerated with the diffusion synthetic acceleration method. The convergence properties of the solver were investigated and compared with the unaccelerated algorithm.

In the first part of the study, a Fourier analysis of the convergence was carried out. Then a 2-D homogeneous system with a stationary fluctuation of the thermal capture cross-section at one location, was considered. The numerical convergence behavior of the accelerated and unaccelerated schemes for neutron noise calculations were demonstrated to be consistent with the theoretical behavior. The diffusion synthetic

acceleration reduces the spectral radius of the solver, although the spectral radius was found to be still quite large (above 0.9). On the other hand, the acceleration is not affected by the number of inner iterations. The results also showed that the convergence rate of the two algorithms decreases as the frequency of the neutron noise source becomes lower.

In the second part, the two schemes were tested on 2-D heterogeneous configurations where the 2-energy group capture cross-sections were perturbed in one fuel cell. If DSA is applied, the number of outer iterations required for convergence reduced by over 20 times. However, the number of outer iterations is still large.

The work is under development and future steps will involve the investigation of a Coarse-Mesh Finite-Difference acceleration method, the extension to a multi-energy group scheme and to 3-dimensional simulations, and the treatment of anisotropic scattering.

ACKNOWLEDGEMENTS

The research leading to these results has received funding from the Euratom research and training program 2014-2018 under grant agreement No. 754316.

REFERENCES

1. C. Demazière, "CORE SIM: A Multi-purpose Neutronic Tool for Research and Education," *Annals of Nuclear Energy*, **38**(12), pp. 2698-2718 (2011).
2. M. Bahrami and V. Naser, "SN Transport Method for Neutronic Noise Calculation in Nuclear Reactor Systems: Comparative Study Between Transport Theory and Diffusion," *Annals of Nuclear Energy*, **114**, pp. 236-244 (2018).
3. A. Rouchon, A. Zoia and R. Sanchez, "A New Monte Carlo Method for Neutron Noise Calculations in the Frequency Domain," *Annals of Nuclear Energy*, **102**, pp. 465-475 (2017).
4. T. Yamamoto, "Monte Carlo Method with Complex-valued Weights for Frequency Domain Analyses of Neutron Noise," *Annals of Nuclear Energy*, **58**, pp. 72-79 (2013).
5. M. Bando, T. Yamamoto and Y. Saito, "Three-dimensional Transport Calculation Method for Eigenvalue Problems Using Diffusion Synthetic Acceleration," *Journal of Nuclear Science and Technology*, **22**(10), pp. 841-850 (1985).
6. Y. Azmy and E. Larsen, "Fourier Analysis of the Diffusion Synthetic Acceleration Method for Weighted Diamond-differencing Schemes in Cartesian Geometries," *Nuclear Science and Engineering*, ***95***(2), pp. 106-115 (1987).
7. A. Zhu, Y. Xu and T. Downar, "Fourier Convergence Analysis of the Infinite Homogenous Multigroup Time-Dependent Boltzmann Transport Equation Using Discrete Ordinates Formulation," *Nuclear Science and Engineering*, **186**(1), pp. 23-36 (2017).
8. M. Adams and E. Larsen, "Fast Iterative Methods for Discrete-Ordinates Particle Transport Calculations," *Progress in Nuclear Energy*, **40**(1), pp. 3-159 (2002).
9. C. Cavarec, J.F. Perron, D. Verwaerde, and J. West, "Benchmark Calculations of Power Distribution Within Assemblies (No. NEA-NSC-DOC--94-28)," Nuclear Energy Agency (1994).
10. A. Mylonakis, H. Yi, P. Vinai and C. Demazière, "Neutron Noise Simulations in a Heterogeneous System: A Comparison Between a Diffusion-Based and a Discrete Ordinates Solver," in *International Conference on Mathematics and Computational Methods applied to Nuclear Science and Engineering - M&C* (2019).